AGU ADVANCING EARTH AND SPACE SCIENCE

Geophysical Research Letters

RESEARCH LETTER
10.1029/2020GL091430

# Three Western Pacific Typhoons Strengthened Fire Weather in the Recent Northwest U.S. Conflagration

**Jacob Stuivenvolt Allen[1], S.-Y. Simon Wang[1], Matthew D. LaPlante[1,2], and Jin-Ho Yoon[3]**

[1]Department of Plants, Soils and Climate, Utah State University, Logan, UT, USA, [2]Department of Journalism and Communication, Utah State University, Logan, UT, USA, [3]School of Earth Sciences and Environmental Engineering, Gwangju Institute of Science and Technology, Gwangju, South Korea

**Key points:**

- Three western Pacific typhoons tracked through the Korean peninsula – with sequential landfall within a two-week period of time
- The diabatic outflow from these typhoons amplified an atmospheric wave train – increasing the pressure gradient over the western U.S.
- The heightened pressure gradient resulted in strong winds, a key element in the rapid spread of fires in Oregon and California

**Supporting Information:**

- Supporting Information S1
- Supporting Information S2
- Supporting Information S3

**Correspondence to:**

J.-H. Yoon,
yjinho@gist.ac.kr

**Citation:**

Stuivenvolt Allen, J., Wang, S.-Y. S., LaPlante, M. D., & Yoon, J.-H. (2021). Three western Pacific typhoons strengthened fire weather in the recent northwest U.S. conflagration. *Geophysical Research Letters*, *48*, e2020GL091430. https://doi.org/10.1029/2020GL091430

Received 27 OCT 2020
Accepted 28 NOV 2020

**Abstract** Strong winds that accentuated a fire outbreak in the western United States in early September of 2020 resulted from an atmospheric wave train that spanned the Pacific Ocean. Days before the atmospheric waves developed in the United States, three western Pacific tropical cyclones (typhoons) underwent an extratropical transition over Korea within an unprecedentedly short span of 12 days. Using a climate diagnostic approach and historical forecast data, it was found that the amplitude of the atmospheric waves accompanying the western U.S. fire weather would not have been so profound if not for the influence of these typhoons. Together, the recurving typhoons provided a significant source of wave activity flux directed toward North America – amplifying the ridge over the U.S. west coast while deepening the trough in central Canada. This anomalous circulation produced the severe frontal system that caused extreme winds in western Oregon, Washington and California – rapidly spreading fire.

**Plain Language Summary** The weather pattern that contributed to rapidly spreading fires in Oregon in early September 2020 can be traced back to an unexpected source: Three typhoons in the western Pacific that ran into the Korean Peninsula within two weeks of each other. Together, Typhoon Bavi, Typhoon Maysak, and Typhoon Haishen each contained enough energy to perturb the jet stream – creating an atmospheric wave train that enhanced the hot, dry weather of the western United States. This study uses forecast models and weather observations to show that these typhoons amplified areas of high and low pressure in North America leading to the intense winds which rapidly spread fire in Oregon, Washington, and California. While the impacts of climate change on these events were not evaluated in this study, the implication is that the effect of weather extremes that are known to be exasperated by climate warming are not always limited to the region in which those extremes occur.

## 1. Introduction

The unprecedented wildfires that intensified rapidly on 7 September 2020, burned over 4,000 km$^2$, contributing to a series of regional conflagrations that killed at least 33 people across the western United States (Newburger, 2020). The remarkable spread of fires occurred in association with an extreme wind event that brought gusts exceeding 22 m s$^{-1}$ to some areas of western Oregon and Washington. Strong down-sloping winds persisted through 8 September 2020, (Figure 1a) and were caused by a powerful frontal system associated with an unseasonably strong east-west pressure gradient (Figures 1b and 1c). Together, the heat-trapping western ridge and the front-producing eastern trough formed a quasi-stationary wave over North America, one that appeared to amplify unexpectedly. Days before, the western North Pacific saw three strong tropical cyclones that passed through the Korean Peninsula in rapid succession: Typhoon Bavi (which reached Korea on August 26), Typhoon Maysak (which reached Korea on September 2), and Typhoon Haishen (which reached Korea and Japan on September 6). All three typhoons had maximum sustained wind speeds greater than 32 m s$^{-1}$ and all of them traveled far enough north to interact with the mid-latitude flow (Figure S1). It was the first time on record that Korea had been hit by three consecutive typhoons within 2 weeks.

It has been established that typhoons interacting with the subtropical jet stream (Jones et al., 2003) can perturb the extratropical flow and trigger high-impact weather events far downstream (Agustí-Panareda et al., 2005; Harr & Dea, 2009; Hodyss & Hendricks, 2010; Pantillon et al., 2013). Archambault et al. (2013) portrayed how a typhoon in the western North Pacific can amplify a high-latitude ridge over western North

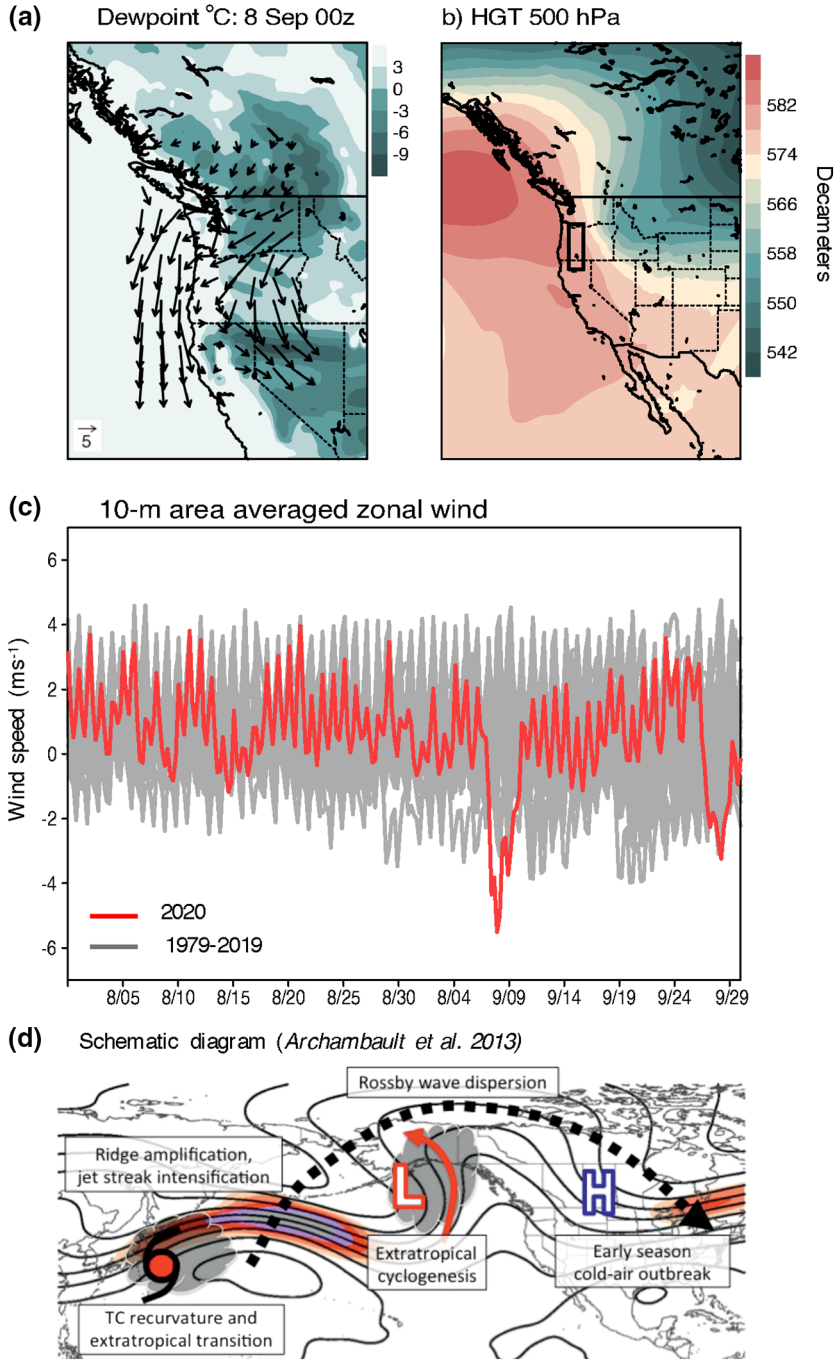


**Figure 1.** (a) Dewpoint temperature (°C) and 10-m winds at the onset of the wind event that rapidly spread fires in Oregon and Northern California. (b) $HGT_{500}$ at the same time, showing a stark pressure-gradient centered over the Pacific Northwest. (c). Area averaged 10-m zonal wind speeds for August through September. The black rectangle in panel b indicates the area used for the area average (124°W–121°W and 41°N–46°N). (d) Schematic diagram illustrating the process in which a recurving typhoon impacts the downstream flow (Archambault et al., 2013).

America, contributing to an early season cold-air outbreak over the central United States (Figure 1d). Mature typhoons and extratropical-transitioning typhoons (Jones et al. 2003) are large sources of diabatic heating. This anomalous heating allows for the advection of low potential vorticity air (PV) into the upper levels of the troposphere (Bosart & Lackmann, 1995; Evans et al., 2017; Grams et al., 2011; Riemer et al., 2008). When a typhoon tracks far enough north to interact with the jet stream, the net result is often a compressed

PV gradient at the location of interaction, and an intensified jet streak to the northeast of a Pacific typhoon (Archambault et al., 2013). Subsequently, downstream extratropical cyclogenesis is enhanced in conjunction with Rossby wave dispersion (Jones et al., 2003; Riemer & Jones, 2010), which amplifies a ridge over western North America (Archambault et al., 2013, 2015; Riboldi et al., 2018). The amplified ridge provides dynamic forcing for a cold-air outbreak east of the Rocky Mountains along with a baroclinic/low-pressure trough. This process is often in sync with the stationary wave regime, amplifying a ridge over the western United States (Archambault et al., 2013; Colle & Mass, 1995).

This situation bears a striking resemblance to what transpired in September 2020, but the extent to which *three* typhoons interacting with the extratropical flows in East Asia contributed to the remarkable North American circulation anomaly is unclear. While a modeling experiment can help diagnose the evolution of this trans-Pacific wave train, conducting an event attribution with fully coupled simulations is difficult. This study uses the National Centers for Environmental Prediction (NCEP) Global Ensemble Forecast System (GEFS) to evaluate members of the model that accurately captured the typhoons and those that did not. It allows us to examine the question: Would the trans-Pacific wave train in early September have been so severe without the upstream impacts of the three typhoons?

## 2. Data and Methods

### 2.1. Observational Analysis

To analyze the interactions each typhoon had with the mid-latitude flow, we adopted a PV framework (Hoskins, 1997) in the non-divergent flow, computing the average 250–150 hPa PV advection to quantify the relative impacts of each typhoon. Additionally, we evaluated the strength of the resulting northward jet streak along with the magnitude of downstream extratropical cyclogenesis, to assess the relative strength and coherence of each typhoon's interaction with the subtropical jet. To collectively look at the downstream impacts of these three typhoons, we computed the Rossby wave activity flux (WAF) using the derivation of Takaya and Nakamura (2001) to depict propagating planetary waves and their associated wave energy in association with the mean background flow. WAF is especially useful for looking at a snapshot of migratory quasi-geostrophic wave disturbances – providing insight on the source and sink of a propagating wave packet (Takaya & Nakamura, 2001). We averaged the 100–300 hPa geopotential height and WAF and plotted their five-day means at three-day intervals, from 25–30 August to 6–11 September. Five-day means were computed to focus on the collective impacts of the typhoons.

Data on the position of each typhoon were gathered from the International Best Track Archive for Climate Stewardship (https://www.ncdc.noaa.gov/ibtracs/) (Knapp et al., 2010). For observational data analysis requiring higher spatial resolution (PV, mean sea level pressure (MSLP), 925 hPa cyclone geopotential height and zonal or meridional wind), we used ERA5 at 6-h intervals (https://climate.copernicus.eu/climate-reanalysis). When comparing ERA5 reanalysis with the GEFS, the ERA5 data are interpolated to a $1 \times 1°$ grid using box averaging to match the GEFS spatial resolution. For broader flow features, namely 250 hPa geopotential height ($HGT_{250}$), we used 6-h NCEP-NCAR Reanalysis (https://psl.noaa.gov/) with a 2.5° spatial resolution from 1948 to 2020 (Cha et al., 2020; Lee et al., 2020; Nakamura et al., 2017; Tu et al., 2009).

### 2.2. Forecast Model Analysis

To evaluate the impact of the typhoons on the trans-Pacific wave train, this study used archived forecast data from the NCEP Global Ensemble Forecast System (https://www.ncdc.noaa.gov). The GEFS is produced four times daily with forecast times out to 16 days after the initialization time. Twenty-one ensemble members at 1° resolution are run in each initialization, with perturbations in the initial conditions gathered from the operational hybrid Global Data Assimilation System 80-member ensemble Kalman filter (Whitaker et al. 2008). We analyzed the archived forecast data that were initialized from 00Z August 18 through 18Z September 3, 2020, in order to provide enough spread for different scenarios. The forecast data evaluated consist of four time steps × 17 days × 21 members, which results in 1,428 possible members for the analysis.

To investigate the effect of the typhoons on the evolution of fire weather conditions, we used an area average of (6° by 6° to account for potential variations in the cyclone center) 1,000-hPa geopotential height ($HGT_{1,000}$) at the typhoon's observed location to determine whether the forecast captured the typhoon. Using $HGT_{1,000}$ is useful because all mature typhoons have an anomalously low value at their center, allowing for a quick evaluation of a forecasted typhoon. We mined at least 24 GEFS initializations (6 days) to select a contiguous window of time that produced roughly equal numbers of positive and negative $HGT_{1,000}$ cases. Typhoons were evaluated during their mature phase because the observational data shows that the jet impacts were present before the typhoon made an extra-tropical transition or dissipated. At this point, a forecast was grouped into the "with" typhoon group if the central pressure was 1 standard deviation below the ensemble mean $HGT_{1,000}$, and into the "without" typhoon group if the central pressure was 1 standard deviation above. Each group contained over 100 ensemble members with the large ensemble size reducing signals not associated with typhoons. Once the typhoons were grouped, the 250 hPa geopotential height ($HGT_{250}$) was compared between the "with typhoon" and "without typhoon" groups, and observations.

## 3. Results and Discussion

### 3.1. Putting the Wind Event into Perspective

The 2-m dewpoint temperature shows that the severe easterly wind associated with the rapidly spreading fires was advecting extremely dry, down-sloping winds into the Northwest (Figure 1a). The direction and intensity of these winds resulted from the negatively tilted ridge/trough pattern over the region – with an amplified pressure gradient driving anomalous downsloping wind speed (Figure 1b). By averaging the 10-m zonal wind field over western Oregon (domain outlined in Figure 1b inset, 123°–121°W, 41°–46°N), we plotted the daily time series of zonal wind for August and September of each year including 2020 (negative value indicates easterly wind). Compared with the 1979–2019 period, the maximum easterly wind occurring on 8 September 2020 is the strongest easterly for this area recorded in the satellite era (Figure 1c). Strong easterly wind causes downslope adiabatic warming/drying that enhances fire weather conditions (Mass & Ovens, 2019). The fact that the early September easterly wind occurred during the climatologically westerly wind regime and at the height of Oregon's fire season is what made the wildfires spread so rapidly. Note that actual (station) wind speeds in Oregon are greater than what the reanalysis data can describe, but the data starting in 1979 are useful for a historical perspective.

### 3.2. Diagnostic Analysis

The response of the jet stream (contours of PV units) to each typhoon (broadly shown by vertical velocity in green shading) and associated PV advection can be seen in Figures 2a–c. Each typhoon resulted in northward jet perturbations which enhanced the local ridge, though Maysak appears to have had the strongest local impact. Subsequently for each typhoon, a zonal jet streak was amplified during the mature and decaying phase of each typhoon. Associated with the jet streak, extratropical cyclogenesis was catalyzed over the north-central Pacific for each typhoon, although the downstream response for Haishen is notably weaker than Bavi and Maysak (Figures 2d–2f). These results are analogous to the mechanisms elucidated by Archambault et al. (2013) and each case resulted in pronounced ridging over the western coast of North America, and a deepened trough over the central continent about four days after the typhoon and jet stream interaction (Figures 2g–2i). Additionally, the peak of Maysak's downstream response occurred at the same time as the Oregon wind event. This suggests that Maysak was the most important typhoon for amplifying fire weather because of its timing and the magnitude of negative PV advection. It is important to note that each typhoon's impact is not limited to a single time step and that this analysis does not show the collective impacts of the typhoons on the mid-latitude flow.

Tracks and temporal spans are shown in Figure 3a – showing that each typhoon's path was independent of the others but the back-to-back barrage of each storm maintained the up-stream jet perturbation show in Figures 2a–2c. All of the typhoons served to maintain an amplified wave train across the north Pacific (Figure 3b). While the storms were temporally adjacent, a supplemental analysis (Figure S2) does not reveal significant impacts of one typhoon on the development or track of another. The cooler sea surface

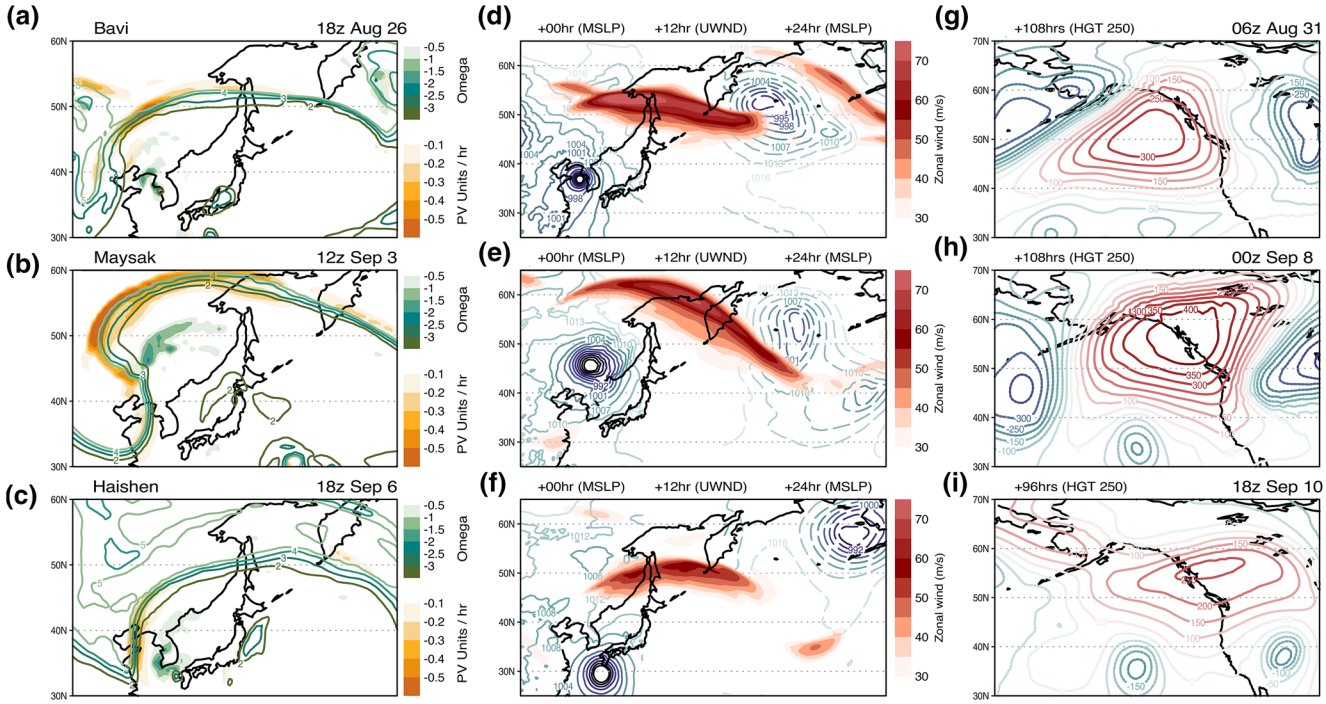


**Figure 2.** (a–c) Potential vorticity units ($10^{-6}$ $m^{-2}$ $s^{-2}$ K $kg^{-1}$) (green contours at 2, 3, and 4 units), potential vorticity advection (orange shading) and vertical ascent (green shading) for typhoon Bavi, Maysak, and Haishen. (d–f) Mean sea level pressure (MSLP) during the mature phase of each typhoon (solid contours), zonal wind at 250 hPa 12 h after the displayed MSLP, and downstream MSLP 24 h (dashed contours) after the date in panel a–c. (g–i) $HGT_{250}$ with the zonal mean removed about four and a half days after the Typhoon time step in panels a–c.

temperatures upwelled after the passing of each storm (Chang et al., 2016) might have served to weaken Haishen, but this typhoon still resulted in downstream effects.

The five-day running means of WAF more adequately shows the collective impacts of the three typhoons. From late August through early September, the source of the WAF continued to increase in the typhoon region through the life cycle of each storm. It generally takes 3 days for a recurving typhoon in the mid-latitude to generate an amplified ridge over western North America (Archambault et al., 2013), and Figure 3b indeed describes such a feature in terms of the WAF propagation. Typhoon Bavi generated an area of significant WAF to its immediate east that amplified the ridge around 150°E (25–30 August in Figure 3b). In the next panel, from 28 August to 2 September, the downstream flow continues to amplify (31 August–5 September). The enhanced ridge over western North America then generated its own WAF in central Canada, deepening the trough there (31 August–5 September). Meanwhile, Typhoon Maysak perturbed the jet stream over east Asia – further amplifying the Aleutian low and the downstream ridge near California. From 3 September to 8 September, Typhoon Haishen repeated the process by strengthening the source and propagation of WAF over the course of five days, making the West Coast ridge and central Canada trough even stronger. This enhanced ridge also contributed to the California heatwave that reached its severity on 6 September, followed by the collapse of cold air that plowed through the Intermountain West in the next two days. While the Oregon wind event was confined to 8 September, Haishen also prolonged ridging after the initial fire spread – maintaining anomalously warm and dry conditions. This episode of cross-Pacific wave train activity was most pronounced from 3–8 September, associated with the heatwave in California and extreme wind events in Oregon.

It is important to note the role of extratropical cyclogenesis (EC) in the ridge-building over the western United States (Bosart et al., 2017; Grams et al., 2013; Archambault et al., 2013). As typhoon Bavi was maturing and tracking toward the Korean Peninsula, EC was developing over the Sea of Okhotsk at 00z 26 August (Figure 2a noted by omega at 55°N and 145°E). Subsequently, Bavi's downstream response was in-phase with the occurring EC. Near 00z on 5 September, EC is once again fundamental to the downstream wave

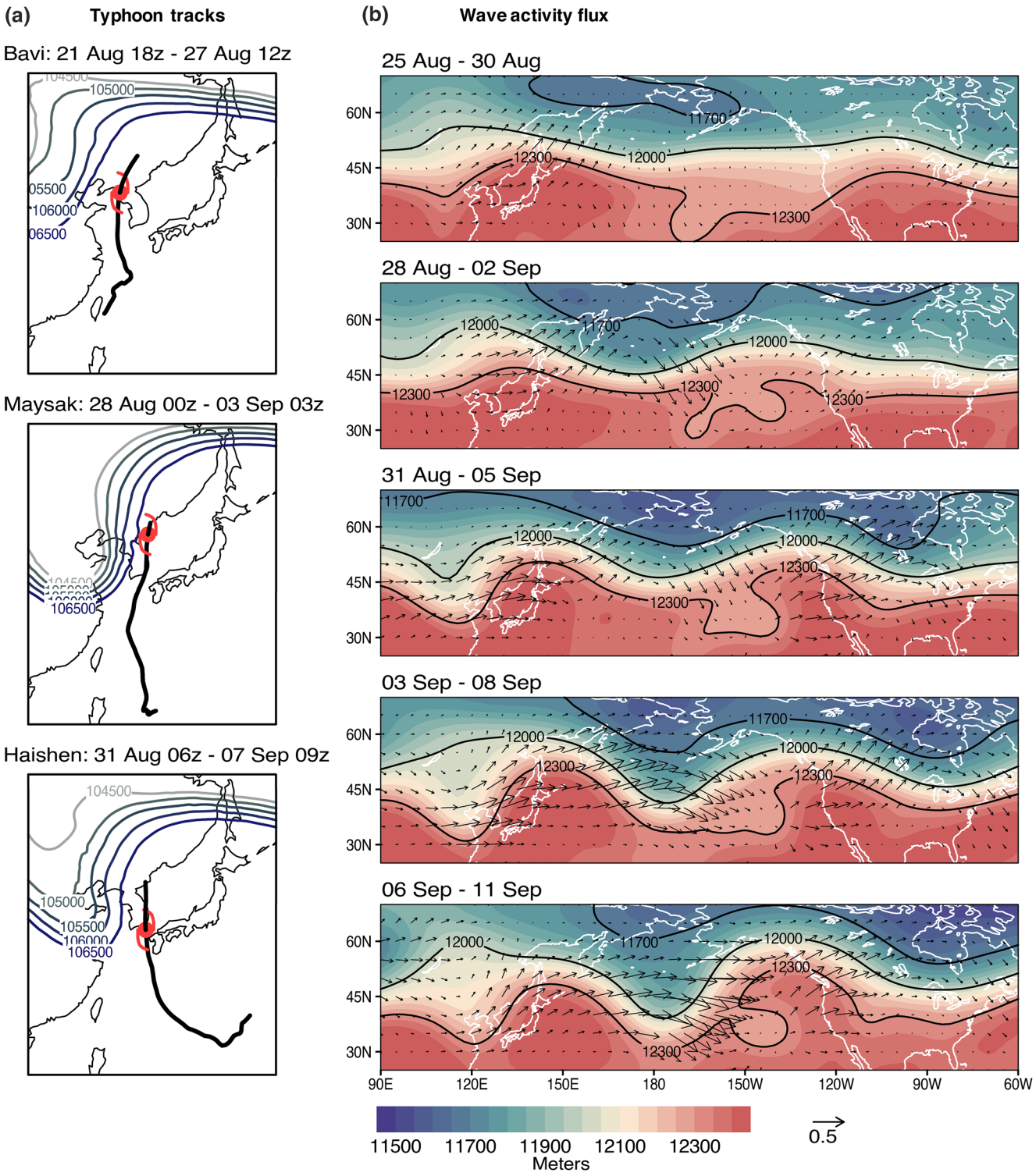


**Figure 3.** (a) Tracks of each typhoon with the $HGT_{250}$ at the last time step that the typhoon was tracked. The tropical cyclone symbol in red indicates the position the storm was last classified as a hurricane by U.S. standards. (b) Average WAF for 5-day periods from 300 to 100 hPa.

amplification – with energetic EC in the north central Pacific (Figure 2e) enhancing the western U.S. ridge (Figure 2f). However, the upper-level WAF source associated with this EC appears to track from East Asia (Figure 3b).

### 3.3. Forecast Data Investigation

Diagnostic analysis using the PV framework and WAF calculation is useful, however, it only depicts the possible source and magnitude of Rossby wave dispersion. It does not identify whether the trans-Pacific wave train would have happened without the western Pacific typhoons. Moreover, atmospheric internal variability can also amplify the trans-Pacific wave train without requiring external forcing like a recurving typhoon (Orlanski & Sheldon, 1995). To account for these unknowns, we used the GEFS 16-day forecasts from 00Z 17 August to 18Z 3 September to provide the closest possible scenarios of the atmospheric circulation with and without the forecast typhoons.

The result of our selection process is a group of GEFS members which accurately captured the position and intensity of the typhoon ("with typhoon"), and a group which missed the typhoon ("without typhoon"). Figure 4 shows the average $HGT_{925}$ field associated with each typhoon compared with observations, showing that this selection process can effectively eliminate the typhoon – and, thus, its subsequent diabatic heating and major influence on the background flow.

Comparing the upper-level circulation associated with each group shows how each typhoon helped amplify the wave train pattern over the North Pacific. The $HGT_{250}$ shown in Figure 5 is a snapshot three to five days after the mature phase of Bavi, Maysak and Haishen. The "with typhoon" $HGT_{250}$ (red contours) depicts enhanced extra-tropical cyclogenesis adjacent to the typhoon and a stronger ridge in western North America accompanied by a slightly deeper trough in the upper Midwest than the "without typhoon" $HGT_{250}$ (black contours). Typhoon Bavi alone (26 August) did not produce a substantial lingering effect on the North American wave pattern after 4 September (Figure S1). However, Typhoon Bavi did contribute to the early September ridge over western North America (Figure 2g, 3a, and 5a) leading to the buildup of hot and dry conditions over the West Coast. For each scenario, the resulting upper-level circulation was more amplified and more representative of observations with the impacts of the typhoons.

For verification purposes, we also evaluated the response of individual members between the with and without typhoons groups. Individual members of the with typhoons group were much more accurate in capturing the observed and amplified $HGT_{250}$ for the time steps leading up to, and during the extreme Oregon wind event (Figure S3). To ensure that this ensemble mean response in the group without typhoons is not the product of noise from our selective sampling, Figure S4 shows the distribution of maximum $HGT_{250}$ for each typhoon and each group – depicting a relatively normal distribution for each group with significant differences between the mean.

We note that the observed circulation pattern over western North America on 8 September is still more extreme than the smoother ridge provided by the with typhoons group (Figure 5b), while the forecast misses the pronounced east-west pressure gradient over the northern Rocky Mountains. Nonetheless, the difference of the trans-Pacific wave train between the two groups is remarkable. The $HGT_{250}$ composite with typhoons clearly depicts the amplified wave train (and high-pressure ridge) that more accurately captures observations (Figure 5c).

## 4. Conclusions

These analyses link two meteorological extremes – connecting the western Pacific typhoon season with impacts on North America's peak fire season. For the catastrophic fire outbreak in early September for western North America, three north Pacific typhoons amplified pre-existing fire-weather and the local pressure gradient – catalyzing an anomalous down-sloping wind event in Oregon. Each typhoon tracked far enough north to perturb the mid-latitude flow – with the quick succession of storms (within two weeks of each other) serving to maintain and continually amplify the downstream circulation. Additionally, our results from the historical GEFS 16-day forecasts combined with reanalysis data support forecast models as a useful

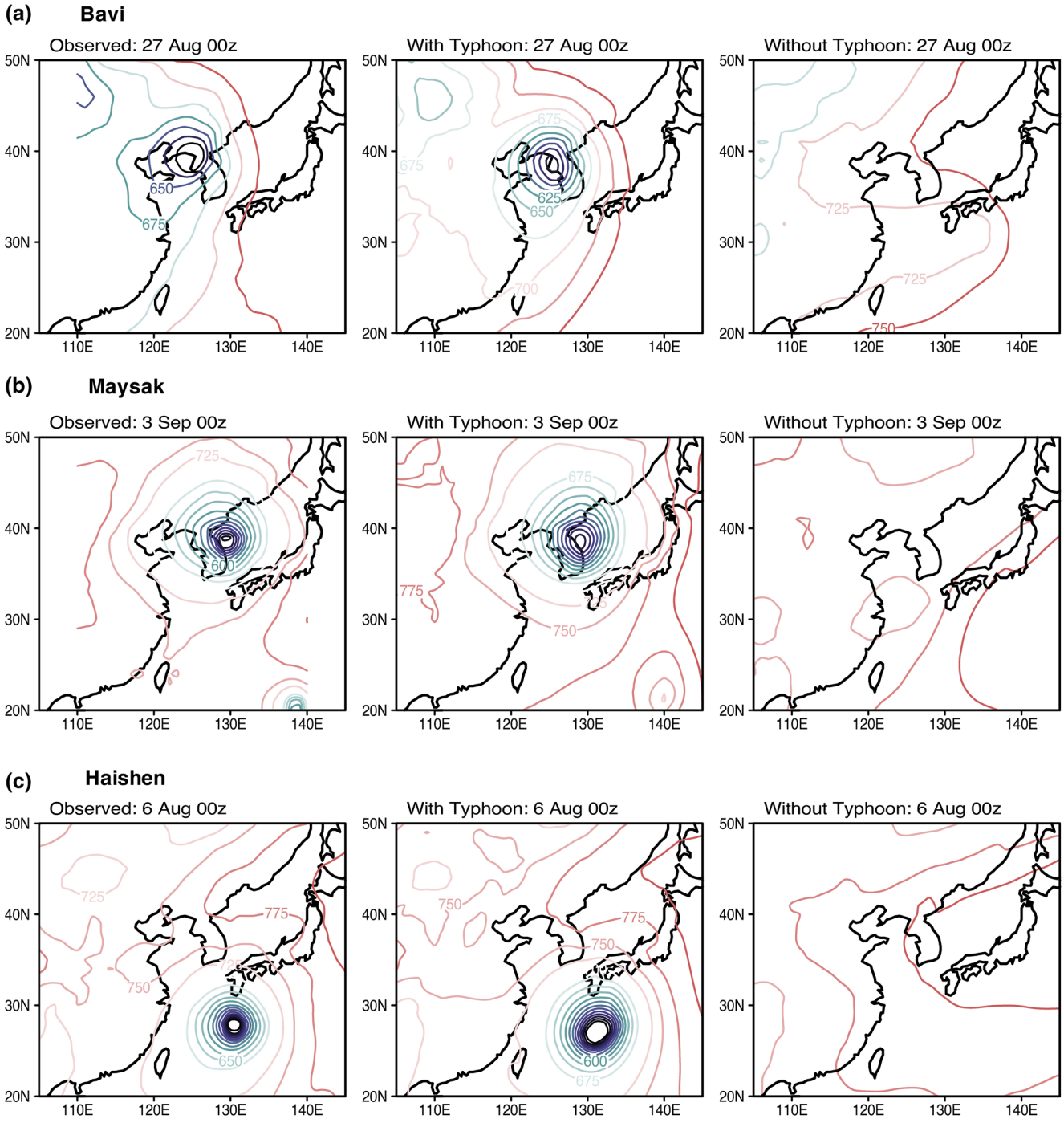


**Figure 4.** (a–c) Typhoons represented by the $HGT_{925}$ field in observations (left panel), the average $HGT_{925}$ of the "with" typhoons group, and the average $HGT_{925}$ of the "without" typhoons group. The number of ensembles in each group is represented as n for each group. The analysis for Bavi is done with the GEFS initialized from 12Z August 18 to 06Z August 24. Maysak's groups are made with initializations from 00Z August 23 to 18Z September 1. Finally, Haishen's groups are composed with initializations from 12Z August 25 to 06Z September 2.

tool for rapid synoptic attribution of extreme weather events. Using this process, we determined the difference between possible atmospheric scenarios for realistic typhoon forecasts and missed typhoon forecasts. The results are analogous to observations and show that the trans-Pacific wave train would have been less amplified, and the fire-associated ridge less robust, without the up-stream impacts of the three typhoons.

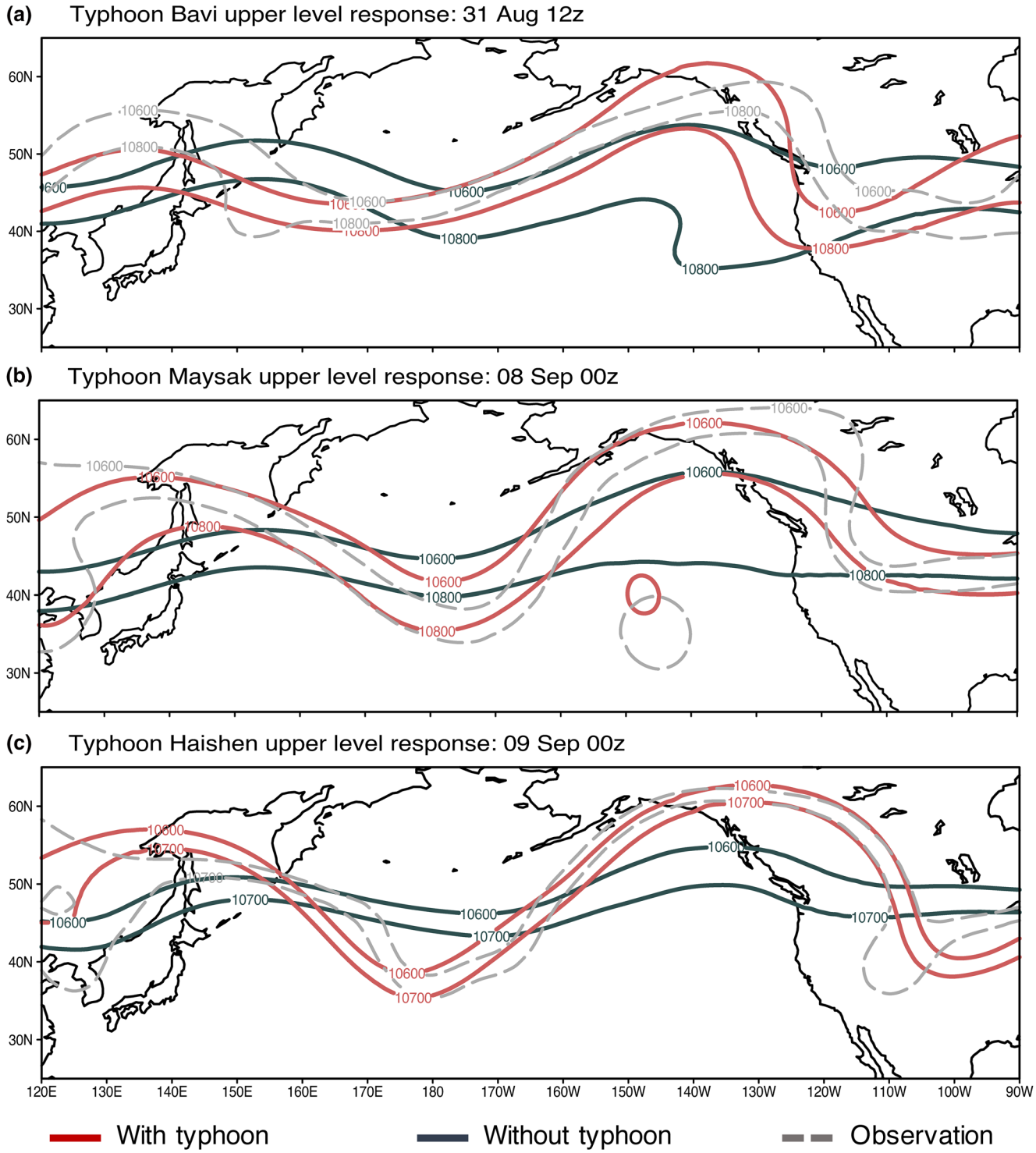


**Figure 5.** $HGT_{250}$ in observations, the with typhoons group, and the without typhoons group for typhoon Bavi, Maysak, and Haishen.

Previous modeling and observational analyses have detailed a northward shift of the typhoon track associated with enhanced greenhouse gas emissions (Oey & Chou, 2016; Sharmila & Walsh, 2018; Wang & Wu, 2019). Further analysis is needed to determine whether or not this shift in the typhoon tracks will accompany an increase in downstream weather perturbations.

## Data Availability Statement

The GEFS is publicly available at https://www.ncdc.noaa.gov/. NCEP reanalysis data are available at https://psl.noaa.gov/(Kalnay et al., 1996) and ERA5 can be found at https://climate.copernicus.eu/(Hersbach et al. 2020). Typhoon tracks are provided by IBTrACS (Knapp et al. 2010).

**Acknowledgments**
The authors acknowledge research funding from the U.S. Department of Energy/Office of Science under Award Number DE-SC0016605 "HyperFACET" and the SERDP project RC20-3056. J.Y acknowledges the KMA R&D Program KMI2020-01115. Thank you to the reviewers for expert guidance and constructive feedback.

## References

Agustí-Panareda, A., Gray, S. L., Craig, G. C., & Thorncroft, C. (2005). The extratropical transition of tropical cyclone Lili (1996) and its crucial contribution to a moderate extratropical development. *Monthly Weather Review*, *133*(6), 1562–1573. https://doi.org/10.1175/MWR2935.1

Archambault, H. M., Bosart, L. F., Keyser, D., & Cordeira, J. M. (2013). A climatological analysis of the extratropical flow response to recurving Western North Pacific tropical cyclones. *Monthly Weather Review*, *141*(7), 2325–2346. https://doi.org/10.1175/MWR-D-12-00257.1

Archambault, H. M., Keyser, D., Bosart, L. F., Davis, C. A., & Cordeira, J. M. (2015). A composite perspective of the extratropical flow response to recurving Western North Pacific tropical cyclones. *Monthly Weather Review*, *143*(4), 1122–1141. https://doi.org/10.1175/MWR-D-14-00270.1

Bosart, L. F., & Lackmann, G. M. (1995). Postlandfall tropical cyclone reintensification in a weakly baroclinic environment: A case study of Hurricane David (September 1979). *Monthly Weather Review*, *123*(11), 3268–3291. https://doi.org/10.1175/1520-0493(1995)123<3268:PTCRIA>2.0.CO;2

Bosart, L. F., Moore, B. J., Cordeira, J. M., & Archambault, H. M. (2017). Interactions of North pacific tropical, midlatitude, and polar disturbances resulting in linked extreme weather events over North America in October 2007. *Monthly Weather Review*, *145*(4), 1245–1273. https://doi.org/10.1175/MWR-D-16-0230.1

Cha, E. J., Knutson, T. R., Lee, T.-C., Ying, M., & Nakaegawa, T. (2020). Third assessment on impacts of climate change on tropical cyclones in the Typhoon Committee Region – Part II: Future projections. *Tropical Cyclone Research and Review*, *9*(2), 75–86. https://doi.org/10.1016/j.tcrr.2020.04.005

Chang, C.-W. J., Wang, S.-Y. S., & Hsu, H.-H. (2016). Changes in tropical cyclone activity offset the ocean surface warming in northwest Pacific: 1981–2014. *Atmospheric Science Letters*, *17*(3), 251–257. https://doi.org/10.1002/asl.651

Colle, B. A., & Mass, C. F. (1995). The structure and Evolution of cold surges east of the Rocky Mountains. *Monthly Weather Review*, *123*(9), 2577–2610. https://doi.org/10.1175/1520-0493(1995)123<2577:TSAEOC>2.0.CO;2

Evans, C., Wood, K. M., Aberson, S. D., Archambault, H. M., Milrad, S. M., Bosart, L. F., et al. (2017). The Extratropical transition of tropical cyclones. Part I: Cyclone evolution and direct impacts. *Monthly Weather Review*, *145*(11), 4317–4344. https://doi.org/10.1175/MWR-D-17-0027.1

Grams, C. M., Jones, S. C., & Davis, C. A. (2013). The impact of Typhoon Jangmi (2008) on the midlatitude flow. Part II: Downstream evolution. *Quarterly Journal of the Royal Meteorological Society*, *139*(677), 2165–2180. https://doi.org/10.1002/qj.2119

Grams, C. M., Wernli, H., Böttcher, M., Čampa, J., Corsmeier, U., Jones, S. C., et al. (2011). The key role of diabatic processes in modifying the upper-tropospheric wave guide: A North Atlantic case-study. *Quarterly Journal of the Royal Meteorological Society*, *137*(661), 2174–2193. https://doi.org/10.1002/qj.891

Harr, P. A., & Dea, J. M. (2009). Downstream development associated with the extratropical transition of tropical cyclones over the western North pacific. *Monthly Weather Review*, *137*(4), 1295–1319. https://doi.org/10.1175/2008MWR2558.1

Hersbach, H., Bell, B., Berrisford, P., Hirahara, S., Horányi, A., Muñoz-Sabater, J., et al. (2020). The ERA5 global reanalysis. *Quarterly Journal of the Royal Meteorological Society*, *146*(730), 1999–2049. https://doi.org/10.1002/qj.3803

Hodyss, D., & Hendricks, E. (2010). The resonant excitation of baroclinic waves by the divergent circulation of recurving tropical cyclones. *Journal of the Atmospheric Sciences*, *67*(11), 3600–3616. https://doi.org/10.1175/2010JAS3459.1

Hoskins, B. (1997). A potential vorticity view of synoptic development. *Meteorological Applications*, *4*(4), 325–334. https://doi.org/10.1017/S1350482797000716

Jones, S. C., Harr, P. A., Abraham, J., Bosart, L. F., Bowyer, P. J., Evans, J. L., et al. (2003). The Extratropical transition of tropical cyclones: Forecast challenges, current understanding, and future directions. *Weather and Forecasting*, *18*, 41.

Knapp, K. R., Kruk, M. C., Levinson, D. H., Diamond, H. J., & Neumann, C. J. (2010). The International Best Track Archive for Climate Stewardship (IBTrACS)Unifying tropical cyclone data. *Bulletin of the American Meteorological Society*, *91*(3), 363–376. https://doi.org/10.1175/2009BAMS2755.1

Lee, T.-C., Knutson, T. R., Nakaegawa, T., Ying, M., & Cha, E. J. (2020). Third assessment on impacts of climate change on tropical cyclones in the Typhoon Committee Region – Part I: Observed changes, detection and attribution. *Tropical Cyclone Research and Review*, *9*(1), 1–22. https://doi.org/10.1016/j.tcrr.2020.03.001

Mass, C. F., & Ovens, D. (2019). The Northern California wildfires of 8–9 October 2017: The role of a major downslope wind Event. *Bulletin of the American Meteorological Society*, *100*(2), 235–256. https://doi.org/10.1175/BAMS-D-18-0037.1

Nakamura, J., Camargo, S. J., Sobel, A. H., Henderson, N., Emanuel, K. A., Kumar, A., et al. (2017). Western North pacific tropical cyclone model tracks in present and future climates. *Journal of Geophysical Research: Atmosphere*, *122*(18), 9721–9744. https://doi.org/10.1002/2017JD027007

Newburger, E. (2020, September 12). *At least 33 dead as wildfires scorch millions of acres across Western U.S. It is apocalyptic. CNBC*. Retrieved from: https://www.cnbc.com/2020/09/12/fires-in-oregon-california-and-washington-spread-death-toll-rises.html

Oey, L.-Y., & Chou, S. (2016). Evidence of rising and poleward shift of storm surge in western North Pacific in recent decades. *Journal of Geophysical Research: Oceans*, *121*(7), 5181–5192. https://doi.org/10.1002/2016JC011777

Orlanski, I., & Sheldon, J. P. (1995). Stages in the energetics of baroclinic systems. *Tellus A*, *47*(5), 605–628. https://doi.org/10.1034/j.1600-0870.1995.00108.x

Pantillon, F., Chaboureau, J.-P., Lac, C., & Mascart, P. (2013). On the role of a Rossby wave train during the extratropical transition of hurricane Helene (2006). *Quarterly Journal of the Royal Meteorological Society*, *139*(671), 370–386. https://doi.org/10.1002/qj.1974

Riboldi, J., Röthlisberger, M., & Grams, C. M. (2018). Rossby wave initiation by recurving tropical cyclones in the western North pacific. *Monthly Weather Review*, *146*(5), 1283–1301. https://doi.org/10.1175/MWR-D-17-0219.1

Riemer, M., & Jones, S. C. (2010). The downstream impact of tropical cyclones on a developing baroclinic wave in idealized scenarios of extratropical transition. *Quarterly Journal of the Royal Meteorological Society*, *136*(648), 617–637. https://doi.org/10.1002/qj.605

Riemer, M., Jones, S. C., & Davis, C. A. (2008). The impact of extratropical transition on the downstream flow: An idealized modelling study with a straight jet. *Quarterly Journal of the Royal Meteorological Society*, *134*(630), 69–91. https://doi.org/10.1002/qj.189

Sharmila, S., & Walsh, K. J. E. (2018). Recent poleward shift of tropical cyclone formation linked to Hadley cell expansion. *Nature Climate Change*, *8*(8), 730–736. https://doi.org/10.1038/s41558-018-0227-5

Takaya, K., & Nakamura, H. (2001). A formulation of a phase-independent wave-activity flux for stationary and migratory quasigeostrophic eddies on a zonally varying basic flow. *Journal of the Atmospheric Sciences*, *58*(6), 608–627. https://doi.org/10.1175/1520-0469(2001)058<0608:AFOAPI>2.0.CO;2

Tu, J.-Y., Chou, C., & Chu, P.-S. (2009). The abrupt shift of typhoon activity in the vicinity of Taiwan and its association with western North Pacific–East Asian climate change. *Journal of Climate*, *22*(13), 3617–3628. https://doi.org/10.1175/2009JCLI2411.1

Wang, R., & Wu, L. (2019). Influence of track changes on the poleward shift of LMI location of Western North pacific tropical cyclones. *Journal of Climate*, *32*(23), 8437–8445. https://doi.org/10.1175/JCLI-D-18-0855.1

Whitaker, J. S., Hamill, T. M., Wei, X., Song, Y., & Toth, Z. (2008). Ensemble data assimilation with the NCEP global forecast system. *Monthly Weather Review*, *136*(2), 463–482. https://doi.org/10.1175/2007MWR2018.1